Fusionlike processes in the ^{14}N+^{232}Th reaction at 30 MeV/nucleon

H. K. W. Leegte, A. L. Boonstra,* J. D. Hinnefeld,[†] E. E. Koldenhof,[‡] R. H. Siemssen, K. Siwek-Wilczyńska,[§]
Z. Sosin,** J. Wilczyński,[††] and H. W. Wilschut
Kernfysisch Versneller Instituut, NL-9747 AA Groningen, The Netherlands
(Received 23 December 1991)

Fusionlike processes were studied in the ^{14}N+^{232}Th reaction at 30 MeV per nucleon. Partition of the fusionlike cross section was determined by detecting nonequilibrium charged particles with an array of phoswich detectors (plastic wall) in coincidence with fission fragments for which the folding angle and thus the momentum transfer was measured. By measuring both single and multiple hits in the plastic wall and by correcting for its incomplete angular coverage a very extensive database of the fusionlike channels was obtained. The results were compared with model predictions comprising the BUU, Fermi jetting, the Boltzmann master equation model, and the nucleon-exchange transport model. It was found that these models which globally describe the dependence of the inclusive momentum transfer in fusionlike reactions cannot account for the associated particle production, in particular if the nucleons bound in the observed complex particles (d,t,α) are included in the comparison. Calculations of the energy spectra of the complex particles with the coalescence formalism indicate that a large fraction of the observed complex particles in the fusionlike reactions cannot be accounted for by pre-equilibrium emission from the fused composite system. They most probably originate from massive-transfer-type reactions that contribute to the beam-velocity component in the energy spectra.

PACS number(s): 25.70.$-$z, 25.70.Jj, 25.70.Lm

I. INTRODUCTION

Complete fusion and quasielastic peripheral reactions almost totally exhaust the reaction cross section in collisions of asymmetric heavy-ion systems at low energies. The clear distinction between these two reaction mechanisms gradually vanishes as the energy is increased. Larger excitation energies generated at increased bombarding energies lead to a strong diversification of peripheral reactions in the form of deep-inelastic processes, massive transfer, and breakup or fragmentation reactions. The fusion reactions, on the other hand, reveal the increasing incompleteness of the fusion process, best manifested in the measurements of the linear momentum of the composite system.

Measurements of the folding angle between fission fragments [1] have been used for many years as a tool for determining the velocity of the fissioning nucleus and, thus, the transfer of momentum in heavy-ion reactions. The folding angle distributions typically exhibit [1–3] a double humped structure with strength concentrated in two regions: at large folding angles corresponding to a small transfer of linear momentum (peripheral reactions), and at smaller folding angles corresponding to nearly full transfer of momentum in the fusion or fusionlike reactions. With increasing bombarding energy the fusionlike maximum in the folding angle distributions gradually shifts from the angle corresponding to full momentum transfer towards larger folding angles [3], i.e., to reactions with incomplete momentum transfer. This has also been observed in the velocity spectra of fusion-evaporation residues [4–6].

The phenomenon of incomplete momentum transfer has attracted much experimental and theoretical interest in recent years. The arresting feature of this phenomenon is the observation that the relative momentum transfer $\langle p \rangle /p_0$ at the same relative velocity of the two colliding nuclei at the barrier is more or less independent of the nucleus-nucleus system studied [6–12]. This systematic behavior can be qualitatively understood if at the same relative velocity the same number of nucleons per projectile mass are emitted with beam velocity in the forward direction. Various models ranging from exciton models [13–15], the Boltzmann master equation [16], and Fermi jetting with and without two-body dissipation [10,17,18] to the intranuclear cascade models with mean field such as the BUU model (e.g., [19,20]) have been used to explain the incomplete momentum transfer. All these models have in common that they only deal with nucleon emission, whereas from incomplete fusion studies it has been known for a long time that the emission of complex particles such as an α particle is important [21,1,22–25].

In spite of much recent effort on the study of the fusionlike processes little quantitative information on the nature and partition of the processes associated with the

incomplete momentum transfer is as yet available. Fast particles observed in reactions contributing to the fusion-like maximum in the folding angle distributions may originate, e.g., from pre-equilibrium emission in central collisions or from massive transfer reactions occurring in more peripheral collisions. It is an open question to what extent emission of light complex particles such as deuterons, tritons, or α particles can be associated with the former mechanism in which the colliding nuclei completely merge and form a composite system. Most previous studies of light particle emission have been inclusive or semi-inclusive, with a moving source decomposition of the particle spectra but no unambiguous identification of the reaction channels [2,24,26,25,27].

In this work we report on a study of the ^{14}N + ^{232}Th reaction at an energy of 30 MeV/nucleon, at which the fusionlike reactions are already dominated by the processes of incomplete transfer of linear momentum [11,3]. We combined the measurements of the folding angle of the fission fragments with detection of nearly all fast charged particles accompanying the fission events. By using a plastic wall in the forward hemisphere for the detection of the charged particles, geometrical biases imposed by coincidence measurements were largely removed. Moreover, by using the fission folding angle method it was possible to quantitatively decompose the fission cross section related to fusionlike and peripheral processes into the various reaction channels.

We have compared our experimental results with predictions of a representative set of current models and theories. The fact that the existing models do not explicitly predict emission of complex particles prevented us from making direct comparisons, but we were able to judge at least the internal consistency of the models. Important in this respect was that we have measured both the incomplete momentum transfer and the associated pre-equilibrium particle emission.

II. EXPERIMENTAL DETAILS

The ^{14}N + ^{232}Th reaction was studied by using a ^{14}N$^{(7+)}$ beam of 420 MeV from the KVI isosynchronous cyclotron. The beam bombarded a ^{232}Th target of 0.55 mg/cm^2 thickness. A schematic picture of the setup is shown in Fig. 1. The fission fragments were detected in two position-sensitive avalanche detectors (PSD) [28] of a sensitive area of 200×140 mm^2, positioned symmetrically on both sides of the beam axis. Each PSD covered the angular range 49° to 110° in the horizontal plane and −27° to +27° in the vertical direction. With a spacing of 2 mm between wires in the PSD's, the direction of the velocity vectors of the fission fragments could be determined with an accuracy of about ±0.3°.

Light charged particles accompanying the fission events were detected in an array of 30 phoswich detectors [29] consisting of a 1-mm-thick fast scintillator (NE102A) and a 50-mm-thick slow scintillator (NE115). The array formed a "plastic wall" that covered the angular range −41° to +41° in the horizontal plane and −29° to +29° in the vertical direction. A solid angle of about 45 msr around the beam axis was not covered by the plastic wall.
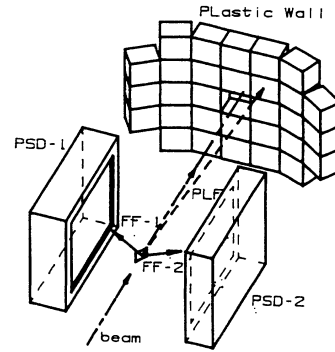

FIG. 1. Experimental setup with position-sensitive avalanche detectors (PSD-1, PSD-2) and 30 phoswich detectors forming the "plastic wall."

The phoswich detectors ensured charge identification of all particles up to $Z = 8$. Mass identification was possible, however, only for the hydrogen isotopes. Energy calibration of the phoswich detectors has been done in a separate experiment [30] by using secondary beams of different reaction products of $1 \leq Z \leq 7$ filtered in a magnetic spectrograph. The response of the detectors was found to be almost linear in energy over their full dynamic range. However, the calibration constants turned out to depend both on Z and A. Except for the $Z = 1$ particles, the dependence on A has been ignored because of the insufficient isotopic resolution. This restricts the energy resolution for the heavier elements to about 10% [30].

The thickness of the front layer (1 mm) of the phoswich detectors determined the energy thresholds below which the particles could not be identified. These thresholds were 9, 12, 15, and 37 MeV for protons, deuterons, tritons, and α particles, respectively. The total thickness of the phoswich detectors (50 mm) determined, in turn, the upper limits for proper particle identification and energy determination. These limits were 77, 106, 127, and 319 MeV for p, d, t, and α particles, respectively.

The $\Delta E, E$ information was obtained in the usual way by separately integrating the analog signal over a short- and long-time gate, respectively, on a charge sensitive ADC. Common gate ADC's were used (FERA [31]). The differences in the gate timing for the events when more than one detector fired were corrected offline. A simple software procedure utilizing the recorded time and energy information was developed for this purpose [30].

III. RESULTS AND DISCUSSION

A. Fission folding angle distributions

In the following we present results of our measurements in which the detection of two fission fragments was used as the event trigger. In order to select a well defined sample of fission events with minimal bias, we gated on a fission fragment in either PSD in a relatively narrow angular window in the azimuthal and out-of-plane angles,

$66° \leq \theta \leq 87°$ and $-7° \leq \phi \leq +7°$, respectively. Thus, as has been checked, the complementary fission fragment always was detected in the opposite detector with nearly 100% efficiency.

For each fission event the folding angle was determined from the two impacts on the PSD's: $\theta_{ff} = \arccos(\mathbf{F}_1 \cdot \mathbf{F}_2)$, where $\mathbf{F}_1$ and $\mathbf{F}_2$ are unit vectors in the direction of the two fission fragments. The upper curve in Fig. 2 shows the folding angle distribution that includes all the accepted fission events, irrespectively of the number and kind of the accompanying charged particles. This distribution is very similar to those measured previously for similar systems at comparable energies [11,32,3,33]. It consists of two components, one at large folding angles corresponding to small transferred momenta, and a second at smaller folding angles corresponding to fusionlike reactions. The two components are separated by a distinct minimum. A possible interpretation of this minimum can be related to the frequently postulated geometrical limita-
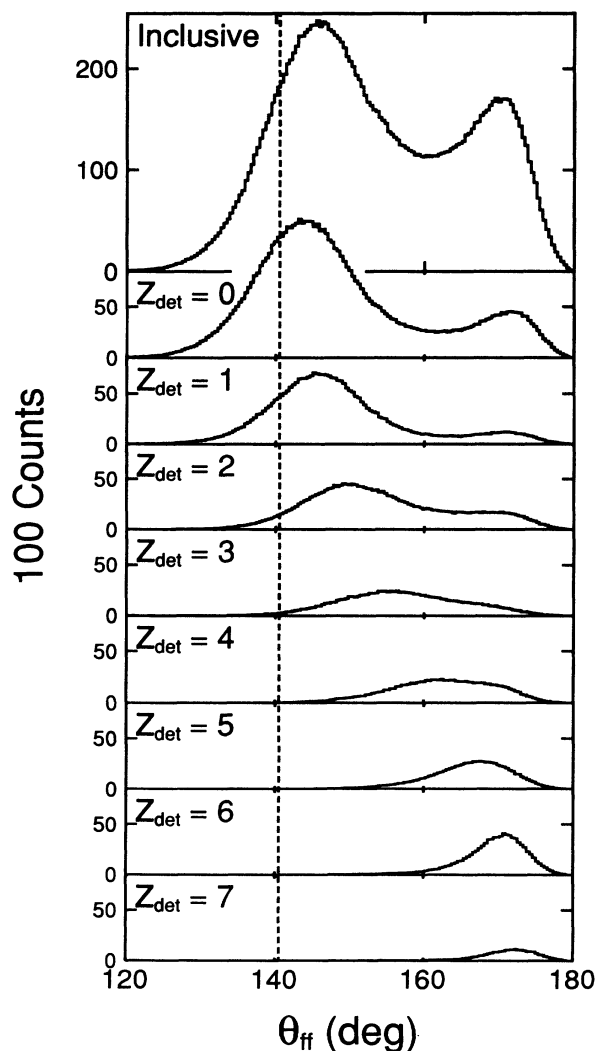
tion of fusion and fusionlike reactions (critical distance [34–36]) on the one hand, and, on the other hand, to a wide class of transferlike peripheral processes involving small momentum transfers at larger impact parameters. If the cross section of these transferlike processes drops monotonically with increasing mass transfer then a minimum in the mass and/or momentum transfer distribution should be observed. The appearance of a minimum is also expected in terms of the breakup-fusion mechanism that enhances asymmetric breakup channels due to much more favored separation energies.

Although the ^{14}N + ^{232}Th system is highly fissile, most likely only the fusionlike part of the folding angle distribution fully represents the respective part of the reaction cross section, while the peak at large folding angle represents only that part of the peripheral reactions which selectively lead to fission. As was shown by Morrissey et al. [37], the fission probability in nonabsorptive reactions approaches unity only after reaching a quite high threshold in the total excitation energy generated in the collision.

By assuming a $1/\sin\theta$ fission angular distribution, the total integrated cross section corresponding to the fusionlike component was estimated to be, $\sigma_{\text{fusionlike}} = 1800$ mb. This value is only slightly smaller than the geometrical cross section of close-impact collisions limited by the distance equal to the sum of the half-density radii, i.e., the "critical distance" that is believed to limit the fusion cross sections at energies well above the Coulomb barrier [34–36].

From the measured folding angle the linear momentum transferred to the fissioning nucleus can be deduced [1], provided the velocity vectors of the fission fragments are known. However, if only the average value of the transferred momentum is of interest, a precise knowledge of the velocities of the fission fragments is not necessary. In that case one can assume symmetric mass division and use the mean value of the kinetic energy $\langle E_k \rangle$ released in each fission event. With this simplifying assumption, the average transferred linear momentum $\langle p \rangle$ relative to the momentum of the incident beam p_0 is given by

$$\frac{\langle p \rangle}{p_0} = \left[\frac{M \langle E_k \rangle}{M_p E_p} \right]^{1/2}$$

$$\times \frac{\sin\theta_{ff}}{[2\sin^2(\theta_{ff} - \theta_1) + 2\sin^2\theta_1 - \sin^2\theta_{ff}]^{1/2}} , \quad (1)$$

where M_p and E_p are the mass and kinetic energy of the projectile, and M is the mass of the fissioning nucleus. For $\langle E_k \rangle$ the updated systematics of Viola [38] were used:

$$\langle E_k \rangle = 0.1189 \frac{Z^2}{A^{1/3}} + 7.3 \text{ MeV} . \quad (2)$$

As one sees from Eq. (1), the folding angle alone does not determine unambiguously the value of the transferred momentum. Apart from θ_{ff}, it is necessary to know the angle θ_1 of the emission of one of the fission fragments with respect to the direction of the velocity of the fissioning nucleus $\mathbf{V}_{fn}$. For fusion or fusionlike reactions the

FIG. 2. Folding angle distributions gated on reaction channels characterized by the combined charge of the detected particles, Z_{det}. The dashed line indicates full momentum transfer.

vector $\mathbf{V}_{fn}$ does not significantly deviate from the beam direction, and therefore θ_1 can be identified with the emission angle of the fragment in the fixed laboratory frame, i.e., measured with respect to the beam direction. This, however, is not correct for peripheral reactions in which the transferred momentum is relatively small. Therefore, the information on the momentum transfer deduced from the folding angle measurements for the peripheral nonabsorptive reactions (appearing as the peak at large folding angles) is less reliable than for fusionlike reactions.

B. Review of the experimental data

Applying relation (1) to the inclusive folding angle distribution (Fig. 2, top), the most probable momentum transfer for the fusionlike reactions is 83%. This result agrees very well with the general systematics [6–12] and, more specifically, with the values found for $^{14}N+^{197}Au$ and $^{14}N+^{238}U$ reactions at the same energy of 30 MeV/nucleon [32,11].

Having a clear *operational* criterion for separating fusionlike reactions from peripheral or nonabsorptive reactions, based on the presence of the distinct minimum in the inclusive folding angle distribution, we will present data on the charged-particle emission separately for these two classes of reactions. The large momentum transfer (LMT) gate, $\theta_{ff} \le 160°$, will refer to the fusionlike reactions, and the small momentum transfer (SMT) gate, $\theta_{ff} > 160°$, to the nonabsorptive (mostly peripheral) reactions.

Figure 3 gives an overview of the energy spectra observed at a forward angle $\theta = 13°$ for various ejectiles emitted in coincidence with fission fragments for the LMT and SMT regions of the folding angle distribution. The spectra are present in an energy per nucleon scale that facilitates for the SMT gate observation of a clear centering of the spectra near the energy corresponding to the beam velocity of 30 MeV/nucleon (indicated by the dotted line). Note that not only projectilelike fragments, but also light particles (p,d,t,α) show this effect. The pronounced beam-velocity peak of α particles for the SMT gate indicates that there are strong contributions from projectile breakup as well as from sequential decays of projectilelike fragments produced in peripheral reactions. Similarly, breakup or transfer-breakup reactions may produce protons, deuterons, and tritons of approximately beam-velocity energies.

The Be events represented by the hatched area in Fig. 3 are due to simultaneous detection of two α particles in the phoswich detector. Most likely they originate from ^8Be produced in the ground state. Since the light output/MeV for Be isotopes is less than for two α particles, the $^8Be_{g.s.}$ events appear to have higher energies.

For the LMT gate (Fig. 3, left) there is a very small chance of observing heavy projectilelike fragments because large transfer of linear momentum has to be coupled, on the average, with a large transfer of mass. As it is seen from the left side of Fig. 3, mostly light ejectiles (p,d,t,α) accompany fission events in the fusionlike reactions. The energy spectra of these particles look different

from those for the SMT gate. The low-energy part is significantly enhanced as compared with the corresponding plots on the right side of Fig. 3. In addition to the expected emission of evaporation- and pre-equilibrium-type particles, both having rather soft exponentially falling energy spectra, we clearly observe within the LMT gate an admixture of fast particles (best seen in the α-particle spectrum) that form a shoulder located at approximately beam-velocity energy.

Figure 4 illustrates the angular dependence of the emission of α particles for both gates in the transferred linear momentum. It is seen that the beam-velocity component, mostly present for the SMT gate, falls off very rapidly with angle. Consequently, at $\theta = 35°$ only the soft component remains. It should be pointed out, however, that this soft component is predominantly of the pre-equilibrium type because it is characterized by a slope parameter of about 40 MeV, while the temperature of the equilibrated compound nuclei is at most 4 MeV.

Figure 5 shows the anisotropy for the emission of light ejectiles and projectilelike fragments with respect to the fission plane. The anisotropy is defined as

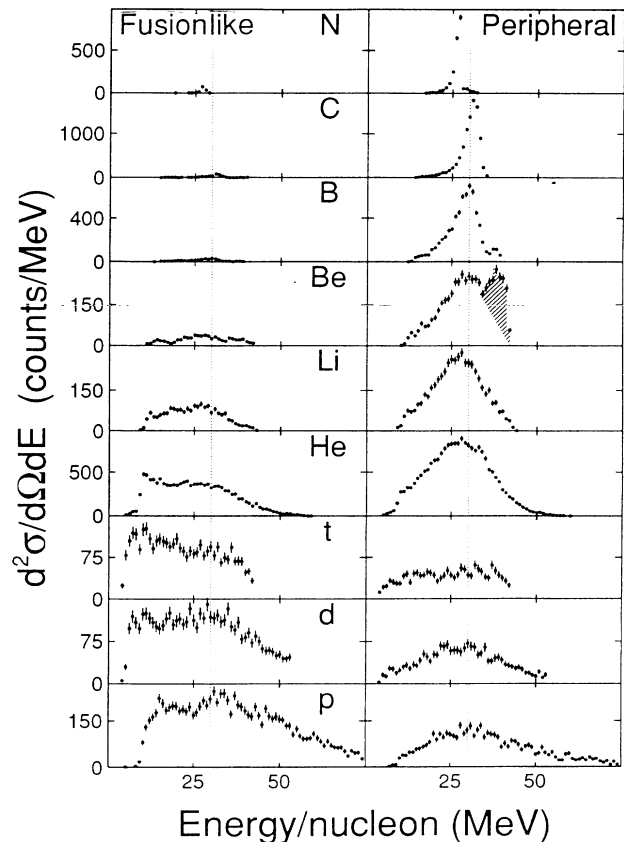$$\mathcal{A} = \frac{Y(\phi=0°) - Y(\phi=90°)}{Y(\phi=0°) + Y(\phi=90°)}, \tag{3}$$

FIG. 3. Energy spectra of various ejectiles of $1 \le Z \le 7$ detected at an angle $\theta = 13°$, and for two gates on the folding angle corresponding to fusionlike and peripheral reactions. The spectra are presented in the energy per nucleon scale. The dotted lines indicate the beam-velocity energy.
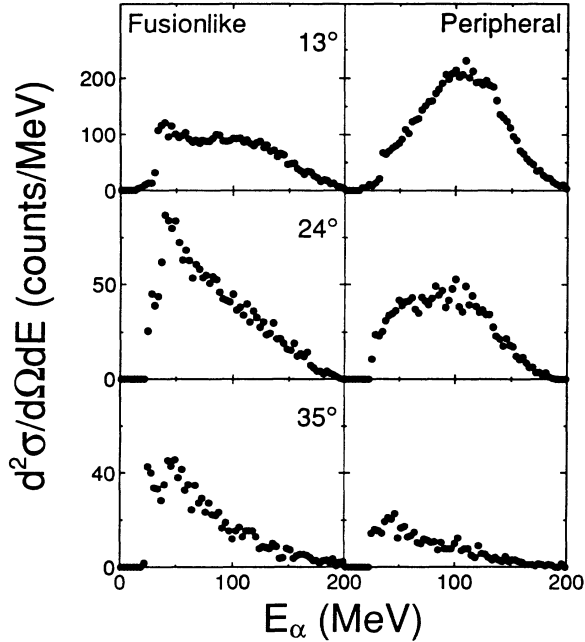
FIG. 4. Energy spectra of α particles at the average angles of 13°, 24°, and 35°, for the LMT (left) and SMT (right), respectively.

where $Y(\phi=0°)$ and $Y(\phi=90°)$ are the yields of the fragments in two detectors placed at the same azimuthal angle $(\theta=13°)$ in the fission plane $(\phi=0°)$ and in the plane perpendicular to the fission plane $(\phi=90°)$, respectively. The anisotropy increases strongly with the mass of the emitted fragment, just indicating that the emission of heavier fragments is associated with more peripheral collisions, larger angular momenta, and, consequently, stronger alignment effects. The observed anisotropies are in qualitative agreement with those observed by Tsang et al. [32] at larger polar angles. In view of the limited granularity of the forward wall and small polar angles covered by the wall, the anisotropy could not be studied
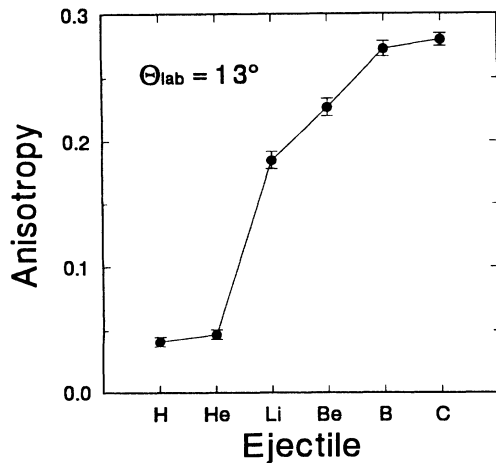

FIG. 5. Anisotropy of the emission of different ejectiles with respect to the fission plane.

in detail as, e.g., in Ref. [39]. The measured anisotropy will be used to determine the "detection efficiency" of the forward detector (see Sec. III D).

C. Partition of the fission cross section

In the following we present more detailed information on the partition of the fission cross section. In Fig. 2, which gives an overview of the measured coincidence data, the folding angle distributions gated by different combinations of charged particles detected in the plastic wall are displayed. Multihit events have been grouped according to the combined Z of the detected particles, Z_{det}, and included in the respective distributions.

From Fig. 2 it can be seen that there is a systematic dependence of the position of the maximum of the folding angle distribution on the transferred charge (or mass). For large transfer of charge/mass (small Z_{det}) the folding angle distributions are dominated by the fusionlike bump, which however, is shifted towards larger angles from the position corresponding to the complete transfer of linear momentum (indicated in Fig. 2 by the dashed line). With increasing Z_{det} the folding angle distributions gradually change their shape and finally become a single maximum at large folding angles (characteristic for peripheral reactions and low transfer of linear momentum).

Apart from complete and incomplete fusion reactions in which only neutrons are emitted, the $Z_{\text{det}}=0$ events of Fig. 2 originate from reactions with emission of charged particles outside the range of the plastic wall. The peak at $\theta_{\text{ff}}=172°$ evidently originates from events in which a massive projectilelike fragment has been emitted into the "hole" in the plastic wall around the beam axis. Also, in the region of the fusionlike bump some of the $Z_{\text{det}}=0$ events may result from undetected light charged particles emitted either at very small angles (into the hole) or at large angles (outside the plastic wall). A quantitative analysis of the effects associated with the incomplete coverage of the emission angles by the plastic wall will be given in Sec. III D.

The results presented in Fig. 2 demonstrate that the fission cross section in the studied reaction is partitioned among a variety of primary reaction channels that cover the full range of mass and charge up to $Z=7$. In Table I the complete information on the partition of the fission cross section for different combinations of charged particles accompanying the fission events is presented. Relative probabilities of about 40 different reaction channels, practically exhausting the entire measured fission cross section and involving charged-particle multiplicities as large as $M=5$, are given. The data are grouped according to the increasing charged-particle multiplicity M and are given separately for the fusionlike $(\theta_{\text{ff}}\leq 160°$, LMT gate) and peripheral $(\theta_{\text{ff}}>160°$, SMT gate) reactions. The sum of the two components is also given. Along with the percentage numbers representing the raw measured results, the values corrected for incomplete coverage of the full solid angle are also presented.

D. Solid-angle corrections of the cross sections

The largest corrections due to the incomplete coverage of the full solid angle are associated with undetected protons, deuterons, and tritons which have the flattest angular distributions and thus the largest probability of being emitted at large angles not covered by the plastic wall. Heavier ejectiles (isotopes of boron, carbon, nitrogen)

have much steeper angular distributions, and therefore the correction for these ejectiles is associated entirely with the hole in the plastic wall around the beam axis. The correction for the detection efficiency leads to a significant redistribution of the relative cross sections. Obviously, the correction affects the reaction channels with the highest multiplicities most severely.

The correction has been made in the following way.

TABLE I. Measured partition (%) of the fission cross section (Meas.) and the partition corrected for incomplete coverage of the full solid angle (Corr.) for fusionlike ($\theta_{ff} \leq 160°$), peripheral ($\theta_{ff} > 160°$), and all reactions.

Emitted particles	Fusionlike Meas.	Fusionlike Corr.	Peripheral Meas.	Peripheral Corr.	Total Meas.	Total Corr.
no charged particle	50.0	27.4	27.5	0	42.4	18.1
p	12.3		4.14		9.54	
d	6.50	25.2	2.11	1.52	4.95	17.2
t	4.41		1.56		3.51	
He	9.93	7.21	10.5	1.11	10.1	5.15
Li	1.44	1.38	2.83	3.00	1.91	1.92
Be	0.488	0.538	3.63	4.14	1.55	1.75
B	0.214	0.369	6.41	14.7	2.30	5.20
C	0.141	0.222	9.40	15.3	3.26	5.30
N	0.082	0.125	2.41	4.01	0.865	1.43
H+H	5.29	13.4	1.34	0.163	3.96	8.97
H+He	4.80	8.65	4.55	1.03	4.71	6.08
He+He	1.28	1.86	5.17	4.13	2.59	2.63
H+Li	0.476	1.10	1.35	2.47	0.772	1.56
H+Be	0.120	0.307	1.32	3.22	0.525	1.29
H+B	0.026	0.091	1.19	4.29	0.420	1.51
H+C	0.013	0.046	0.673	1.63	0.235	0.578
H+N	0.009	0.031	0.041	0.100	0.020	0.054
He+Li	0.198	0.346	2.31	5.99	0.909	2.25
He+Be	0.044	0.099	1.73	5.15	0.611	1.80
He+B	0.008	0.025	0.498	2.01	0.174	0.695
He+C	0.003	0.008	0.049	0.128	0.019	0.049
He+N	0.005	0.013	0.007	0.019	0.006	0.015
H+H+He	0.874	3.97	1.29	1.64	1.02	3.18
H+H+H	0.624	3.78	0.211	0.166	0.484	2.56
H+He+He	0.400	1.39	2.62	5.89	1.15	2.91
He+He+He	0.049	0.130	1.39	4.37	0.501	1.56
H+H+Li	0.052	0.270	0.286	1.05	0.131	0.535
H+H+Be	0.010	0.064	0.185	0.735	0.069	0.291
H+H+B	0.002	0.014	0.058	0.315	0.021	0.116
H+He+Li	0.037	0.148	0.745	3.53	0.275	1.29
He+He+Li	0.005	0.018	0.298	1.65	0.104	0.568
H+H+H+He	0.068	0.684	0.195	0.638	0.111	0.669
H+H+He+He	0.039	0.326	0.452	2.02	0.179	0.897
H+H+H+H	0.040	0.522	0.026	0.061	0.035	0.366
H+He+He+He	0.008	0.054	0.321	1.70	0.113	0.609
He+He+He+He	0	0.002	0.030	0.169	0.010	0.058
H+H+H+Li	0.002	0.030	0.022	0.148	0.009	0.070
H+H+He+Li	0.002	0.017	0.068	0.506	0.024	0.182
H+H+H+H+He	0.003	0.075	0.012	0.077	0.006	0.076
H+H+H+H+H	0.002	0.055	0.002	0.015	0.002	0.041
H+H+H+He+He	0.001	0.021	0.033	0.233	0.012	0.092

The angular distribution for each ejectile of different Z was extrapolated beyond the range of the plastic wall for both very small (near the beam direction) and large angles. The anisotropy of the distributions in the azimuthal angle (due to the correlation with the fission fragments) also was taken into account. The ratio of the number of particles of given Z detected in the plastic wall to the total number obtained from the extrapolation was taken as the average detection efficiency ϵ_z of ejectiles of charge Z.

It was found that for fusionlike reactions the efficiencies ϵ_z for H and He particles do not significantly depend on the reaction channel, i.e., the number and kind of other accompanying charged particles. Consequently, it was assumed that the emission of the light ejectiles is uncorrelated. The probability for observing a given reaction channel j characterized by the emission of several particles of the same or different Z can then be factorized. Since some of the particles escape detection (with the probability $1-\epsilon_z$), the probability $\mathcal{P}_{ij}(Z)$ of detecting $n_i(Z)$ particles of type Z out of the emitted $n_j(Z)$ is given by the binomial expression

$$\mathcal{P}_{ij}(Z)= \begin{bmatrix} n_j(Z) \\ n_i(Z) \end{bmatrix} \epsilon_z^{n_i(Z)}(1-\epsilon_z)^{n_j(Z)-n_i(Z)} \ . \tag{4}$$

The probability for channel j to appear as channel i is then given by the product of the individual probabilities for each value of Z in channel j,

$$\mathcal{P}_{ij}= \prod_Z \mathcal{P}_{ij}(Z) \ . \tag{5}$$

The observed yield of a given reaction channel i, N_i^{obs}, has to be corrected for the contributions from all other channels j appearing as channel i when some of the charged particles escaped detection in the plastic wall. Using expression (4), one can solve a set of coupled equations,

$$N_i^{\text{obs}}= \sum_j \mathcal{P}_{ij}N_j \ , \tag{6}$$

and find the primary yields N_j corrected for the incomplete coverage of the full solid angle:

$$N_j= \sum_i \mathcal{P}_{ij}^{-1}N_i^{\text{obs}} \ . \tag{7}$$

As mentioned above, the basic assumption of the uncorrelated emission is well justified for light ejectiles (H, He) in the fusionlike reactions (LMT gate) (cf. [40]). In the case of emission of heavier ejectiles (Li, Be, B, C, N), which mostly appear in the SMT gate (peripheral reactions), the validity of this assumption could not be checked directly. Nevertheless, we have used the same method of determining the detection efficiency ϵ_z and the probability $\mathcal{P}_{ij}$ for all reaction channels involving also heavier ejectiles. It was important, however, to perform the yield redistribution calculation separately for the fusionlike and peripheral reactions. This is obvious because in peripheral reactions (SMT gate) the light charged particles originate mostly from breakup and/or transfer-breakup reactions and consequently have steeper angular distributions than in the case of fusionlike reac-

tions (see Fig. 4).

The factorization procedure is in apparent contrast with the well-known fact that a large fraction of the reaction channels may involve the emission of projectilelike fragments in unbound states and thus undergoing sequential decay [41–43]. However, corrections of this nature will introduce systematic errors in the present procedure only for very small relative energies, as in the case of emission of ^{8}Be$_{\text{g.s.}}$ [44].

Our method of correction for the incomplete coverage of the full solid angle much benefits from the fact that the extrapolations have to be contained within the total number of fission events. This feature of "unitarity" of the problem reduces the evaluation of the corrections to a redistribution of the yields of different channels within the fixed total number of fission events. For example, in the case of peripheral reactions with emission of projectilelike fragments at very small angles, the steep angular distributions, and thus uncertain extrapolations, can be jointly normalized to the number of $Z_{\text{det}}=0$ events in the peak at large folding angles (see Fig. 2).

Only for $M=1$ events were the isotopes of hydrogen (p,d,t) treated separately in the procedure of the cross section redistribution. For all other reaction channels the H isotopes were taken jointly. It is seen from Table I that the effect of the redistribution of the cross section is significant. Especially for reaction channels of high multiplicity the corrections are very large and reach a factor of 20 for $M=5$. However, the corrected cross sections for these channels are still very low as compared with reactions of lower multiplicity. (See the multiplicity distribution presented in Fig. 6.) Clearly, the observed reactions are dominated by low charged-particle-multiplicity events. The average charged-particle multiplicity, corrected for the incomplete coverage, is $\langle M \rangle=1.2$; the uncorrected value was $\langle M \rangle=0.7$. About 90% of the fission cross section, for both fusionlike reactions and peripheral reactions, corresponds to the events in which at most two charged particles are emitted in addition to the fission fragments.

Table I summarizes the information on the partition of the cross section of the fusionlike reactions. Comparable
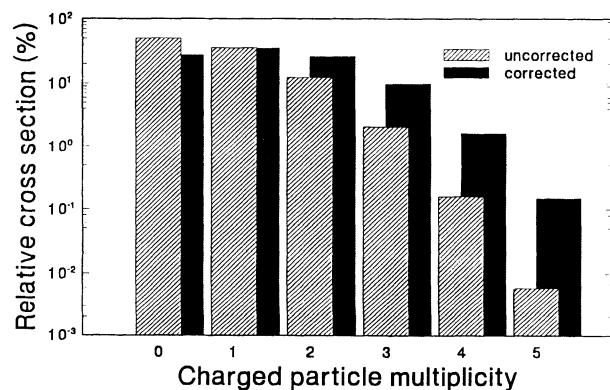

FIG. 6. Multiplicity distribution of charged particles before (hatched) and after (darkened) the correction procedure. Note the logarithmic scale.

information has been obtained so far only for the ^{28}Si$+^{100}$Mo reaction at 700 MeV by Chbihi *et al.* [45], although it has not been corrected for the detection efficiency. In spite of the rich variety of reaction channels listed in the table, there are only several channels that practically exhaust the entire yield in the folding angle distribution. These channels are $xn+f$, $1H+f$, $1\alpha+f$, $2H+f$, $H+\alpha+f$, $2H+\alpha+f$, and $3H+f$. Together, they comprise more than 1400 out of 1800 mb of the angle-integrated fusionlike cross section. Figure 7 shows the partition of these channels. It should be noted that the percentage of the $xn+f$ channel (27%) representing fission events without emission of charged particles is overestimated. This is due to discrimination against slow charged particles which stopped in the ΔE layer of the phoswich detectors. We have found that allowing for all charged particles, even those stopped in the ΔE layer and thus poorly identified, the percentage of the $xn+f$ channel for fusionlike reactions decreases to 15%. This estimate corresponds to the extrapolation of angular distributions based on the trends observed at forward angles. No flattening of the angular distributions indicating the presence of an evaporation component from the combined system was observed in that angular range.

In Sec. V the results of Table I will be compared with pre-equilibrium models. For this reason it is still necessary to obtain some indications of the magnitude of the evaporation contribution averaged over all fusionlike channels. An upper limit was determined in the following way. The average momentum transfer is 83%; therefore it is assumed that on the average a compound nucleus is formed due to the fusion of ^{12}C$+^{232}$Th, while one proton and neutron are emitted with beam velocity (this corresponds to 86% momentum transfer). The temperature of the compound would then be 3.1 MeV. Using Coulomb barriers of 12 MeV for p,d, and t and 24 MeV for α particles, the Maxwellian spectra of the evaporated particles are calculated in the moving frame of the compound nucleus and integrated over the angular range of the forward wall. The resulting spectra are compared to the angle-integrated experimental spectra, with the requirement that the calculated spectrum cannot exceed the experimental yield (the experimental spectra are shown in Secs. V B and V C). In this way an upper limit
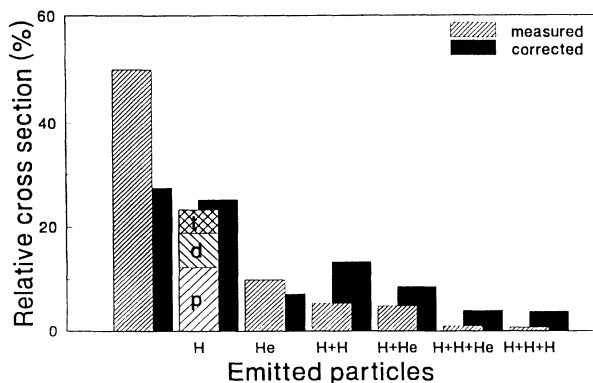
for evaporation of 14% is obtained for protons, whereas for α particles a contamination less than 1% is found. This large difference is mainly due to the experimental thresholds of 9 MeV for protons and 37 MeV for α particles, which are below and above the Coulomb barrier, respectively. Note that this estimate depends little on the assumptions concerning momentum transfer and temperature. For example, using full momentum transfer and a maximum temperature of 3.4 MeV would change the upper limit for the proton evaporation contamination to 16%.

IV. CHANNEL DEPENDENCE OF THE MOMENTUM TRANSFER

The folding angle distributions for all channels listed in Table I have been analyzed separately. For each reaction channel, the *most probable* value of the transferred momentum $\langle p \rangle$ has been determined from the position of the maximum in the folding angle distribution by using Eq. (1). The deduced values $\langle p \rangle$, relative to the incident momentum p_0, are displayed in Fig. 8 as a function of Z_{det} and the charged-particle multiplicity M. In a few cases, when two or more different reaction channels have the same multiplicity M and the same summed Z, a weighted average has been displayed. The transferred linear momentum increases systematically with the transferred mass (charge). The solid line in Fig. 8 represents the predicted dependence of the transferred linear momentum on the transferred mass, assuming that the remaining fragment(s), having the combined mass number $2Z_{det}$, move with beam velocity. The charge binary reactions of $M=1$ (indicated in Fig. 8 by solid circles) and the $M=2$ events (shown by pluses) are the best candidates for following this dependence. The dashed line shows an approximate limit corresponding to a "soft-pre-equilibrium" emission of Z_{det} protons and Z_{det} neutrons in the direction of the forward wall. It was assumed that the "softly" emitted pre-equilibrium protons and neutrons have the same energy spectra as those calculated for the compound-nucleus emission, but with a forward-peaked angular distribution. We would like to call attention to the fact that a large momentum transfer (close to the limit indicated by the dashed line in Fig. 8)
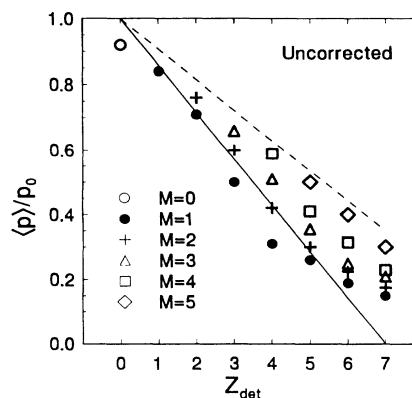
FIG. 7. The cross-section distribution of the main channels of fusionlike reactions.

FIG. 8. Measured transferred momentum vs detected charge, partitioned according to multiplicity M.

can be reached not only via emission of particles from a precompound composite system (we reserve the term *pre-equilibrium* emission for these processes), but also via deep-inelastic, i.e., completely damped, reactions. Since a projectilelike product of deep-inelastic interaction is usually highly excited, it eventually disintegrates into several light particles. The upper limit of the momentum transfer in such damped-fragmentation reactions lies even above the dashed line.

It can be noticed in Fig. 8 that with an increasing number of emitted charged particles carrying away a fixed value of the combined charge Z_{det}, the transferred linear momentum increases. This means that the events of higher charged-particle multiplicity, on the average, represent reactions with a higher degree of equilibration. Note, however, that only the data points corresponding to the highest multiplicities tend to approach the limit of the forward-directed soft-pre-equilibrium emission or damped-fragmentation reactions.

The magnitudes of the transferred linear momentum are also influenced by the incomplete coverage of the full solid angle, in a similar way as the channel yields discussed above. By using the same matrix $\mathcal{P}$ as defined by expression (5), the correct values $\langle p_j \rangle$ have been determined as

$$\langle p_j \rangle = \frac{\sum_i \mathcal{P}_{ij}^{-1} N_i^{obs} \langle p_i^{obs} \rangle}{\sum_i \mathcal{P}_{ij}^{-1} N_i^{obs}} , \tag{8}$$

where N_i^{obs} and $\langle p_i^{obs} \rangle$ denote the uncorrected yields and measured *average* linear momenta, respectively, for channels identified as channel i. Because $\mathcal{P}$ is defined separately for the LMT and SMT gates, the procedure has been applied for each of the two gates and the weighted average has been taken as the corrected value of $\langle p_j \rangle$. In Fig. 9 the corrected values are presented. It is seen from a comparison of Figs. 8 and 9 that the corrected values of the transferred momentum for a given value of Z_{det} are generally larger. (This effect is probably overestimated because we assumed that the undetected particles carried away the same average momentum as the particles detected in the forward wall.) For many channels the data points approach or even slightly surpass the limit of soft-pre-equilibrium emission. Taking into account the
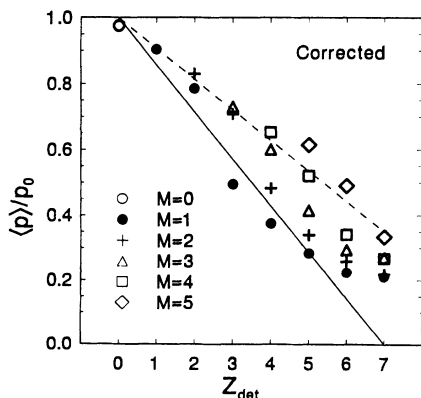

FIG. 9. Same as Fig. 8, but corrected for incomplete coverage of the full solid angle by the particle detectors.

fact that in the damped reactions the upper limit of the momentum transfer for a given Z_{det} value is even somewhat higher than that indicated by the dashed line in Fig. 9, it is plausible that the high-multiplicity events (viz., $M = 4$ and 5) indeed originate from the "multifragmentation" processes following completely damped reactions. Remembering, however, the uncertainties in the calculation of the corrected momentum transfer, we cannot draw firm conclusions concerning the reaction mechanism based on the observed momentum transfer alone.

V. COMPARISONS WITH THEORETICAL PREDICTIONS

A. Transfer of linear momentum and pre-equilibrium multiplicities

Several theoretical models attempt to describe the dynamics of nucleus-nucleus fusion processes at low and intermediate energies. At low energies, the one-body dissipation mechanism is believed to play the essential role. In this mechanism the projectile nucleons entering the target are captured when they cannot escape from the mean field of the target nucleus, while projectile nucleons with energies larger than $\epsilon_F + E_B$ will escape from the target. If the nucleons escape due to the coupling of the Fermi velocity in the donor nucleus with the relative velocity of the colliding nuclei, then the emission process is called *Fermi jetting*. Since the Fermi energy ϵ_F and the binding energy of a nucleon, E_B, are nearly independent of the nuclear mass, the incomplete momentum transfer associated with this mechanism is expected [10] to be a universal function of the beam velocity and independent of the colliding system. A simple model applying the window-wall dissipation formula has been proposed by Möhring, Swiatecki, and Zielinska-Pfabé [17] in order to describe both Fermi-jetting and one-body dissipation. A similar model has been proposed by Randrup and Vandenbosch [18] that is an extension of the nucleon-exchange transport model (NET) and also incorporates the reduction of jetting due to nucleon-nucleon collisions [46], as will be discussed below.

With the decreasing role of Pauli blocking at higher energies, nucleon-nucleon collisions become important, and thus two-body dissipation sets in. Consequently, more momentum is transferred than predicted by the jetting mechanism. Two-body dissipation is the basic mechanism underlying various versions of the exciton model [47,13–15]. The Boltzmann master equation (BME) approach has been extended by Blann [16] for heavy-ion-induced reactions. The model describes the time evolution of particle-hole excitations in the composite system and allows emission of nucleons into the continuum during the relaxation process.

Various intranuclear cascade models can be applied at high energies. A simple leading-particle formula has been proposed by Natowitz *et al.* [48] in order to explain the systematics of linear momentum transfer even in the low-energy regime (above 20 MeV/nucleon).

The most complete dynamical picture of nucleus-nucleus collisions is offered by the BUU approach, which

attempts to describe the time evolution of one-particle density distribution in full phase space. Both one- and two-body dissipation play a role (cf. [19]). However, similarly to the models mentioned above, the BUU describes only nucleon emission and predicts event-averaged values. Therefore, for example, the average multiplicity of pre-equilibrium nucleons can be predicted, but not the multiplicity distribution or, more important, the emission of complex particles. We have not attempted to compare to the QMD [49,50] or QPD [51] models because they require a large computational effort. So far the only result for an asymmetric system at low energy ($^{14}N + ^{154}Sm$ at 35 MeV/nucleon) has been reported in Ref. [51] which seriously underpredicts the α-particle production.

We start the discussion with a comparison of the average nucleonic characteristics of fusionlike reactions. We interpret the entire $\theta_{ff} \leq 160°$ bump in the folding angle distribution as representing fusionlike reactions. This interpretation is supported by the fact that the magnitude of the total cross section of this component, $\sigma_{fusionlike} = 1800$ mb, is close to the value of the fusion cross section predicted by the critical-distance model [34–36]. Also for the BUU calculations, discussed more extensively later, we find for the studied system that the fusionlike reactions persist up to an impact parameter $b = 8$ fm ($\sigma_{fusionlike} = 2000$ mb). For $b > 8$ fm, first deep-inelastic reactions and then quasielastic reactions are predicted. Taking the above arguments into account, it is justified to include all events below the minimum in the folding angle distribution ($\theta_{ff} \leq 160°$) for comparison with the theoretical predictions.

There are four quantities that the existing models can predict and that can be deduced from our experiment for a comparison. They are the cross section $\sigma_{fusionlike}$, the average momentum transfer $\langle p \rangle / p_0$, and the average proton and neutron multiplicities corresponding to pre-equilibrium emission $\langle M_p^{pre} \rangle$ and $\langle M_n^{pre} \rangle$. In order to be abe to compare the various models to our data we have to convert the experimental data to event-averaged values, taking into account the emission of both nucleons and complex particles. (Alternatively, one may construct from theoretical density distributions the expected characteristics of complex particles, for example, by using the coalescence prescription that we will discuss later.) Protons and neutrons bound in the complex particles have to be included for the determination of the average proton and neutron multiplicity, i.e.,

$$\langle M_p^{pre} \rangle = \sum_i n_i \frac{\sigma_i}{\sigma_{fusionlike}} , \qquad (9)$$

where n_i is the number of protons (bound in complex particles and/or unbound) associated with channel i as listed in Table I. For neutrons we can only provide the bound-neutron multiplicity $\langle M_n^{pre} \rangle_{bound}$. The missing information on the multiplicity of unbound neutrons has been estimated from experimental systematics that were obtained by compiling existing data [52–56]. The systematics are shown in Fig. 10, which presents the pre-equilibrium neutron multiplicity per projectile nucleon as
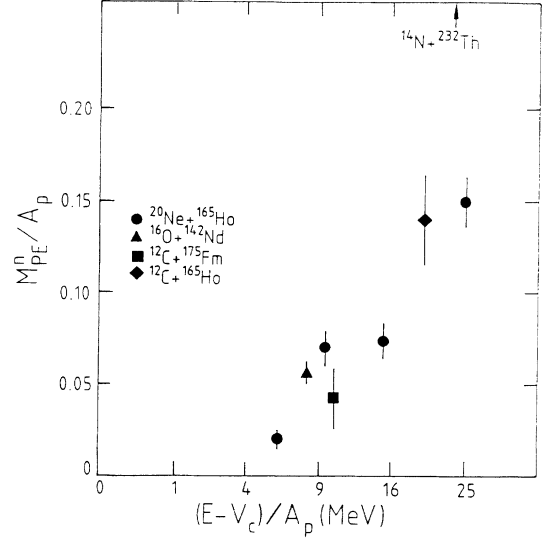

FIG. 10. Systematics of the multiplicity of the pre-equilibrium neutrons in fusion reactions based on the data from Refs. [52–56]. The multiplicity per projectile nucleon is plotted as a function of the energy per nucleon at the contact configuration. Note the quadratic scale of the energy.

a function of the relative velocity at the contact configuration (note the quadratic scale). The data points represent the average multiplicities obtained from a moving-source analysis of neutron spectra gated on fusionlike reactions. It is seen from Fig. 10 that the average multiplicity of pre-equilibrium neutrons per projective mass increases almost linearly with the relative velocity of the colliding system. From the systematics we obtain for the present reaction a value $\langle M_n^{pre} \rangle = 2.1$ for unbound neutrons. The experimental values of the cross section, average transfer of linear momentum, and average multiplicities $\langle M_n^{pre} \rangle$ and $\langle M_p^{pre} \rangle$ are listed in Table II together with the predictions of the models mentioned at the beginning of this section. As noted in Sec. III D, the data could be contaminated by up to 14% evaporated protons, which would lower the values for $\langle M_p^{pre} \rangle$ with 0.1 nucleon. Some details concerning the model calculations are given in the Appendixes.

It is seen from Table II that the BME model of Blann [16] and the leading-particle formula of Natowitz *et al.* [48] predict the average value of the momentum transfer to be close to or below the experimental result. It should be noted, however, that in both models the large missing momentum, to some extent, is a consequence of the assumption that the escaping particles are emitted at small angles $\langle \theta \rangle \simeq 20°$ [57–59]. In contrast, the other three models listed in Table II predict that the transverse momenta of the escaping particles can be quite large. Since BME and the leading-particle formula underpredict the momentum transfer, there is no room in these models, which only deal with nucleons, for the additional emission of pre-equilibrium complex particles. Therefore, the presence of complex particles has to be explained on basis of, e.g., coalescence of the pre-equilibrium nucleons to obtain consistency with the experimental observations.

TABLE II. Comparison of different theoretical predictions with experimental results.

	Ref.	(σ_{ff}) (b)	$\langle p \rangle/p_0$ (%)	$\langle M_p^{pre} \rangle$ Unbound	Bound^a+ unbound	$\langle M_n^{pre} \rangle$ Unbound	Bound^a+ unbound
Experiment	This work	1.8	83	0.5	1.7	2.1^b	3.5
Fermi jetting	[17]	2.1	90	0.3		1.7	
Extended NET^c	[18]	2.1	96	0.6 (0.2)		2.7 (1.1)	
BME	[16,3]		75	0.6		2.6	
Leading particle	[48]		82	0.8		2.6	
BUU	[20]	2.0	90	1.3		1.6	

^{a}Comprises complex particles.
^{b}Estimated from Fig. 10.
^{c}The values in parentheses are for (forward) projectilelike jetting.

However, both models underpredict the number of bound plus unbound nucleons.

The remaining models (Fermi jetting [17], NET [18], and BUU [20]) overpredict the momentum transfer. In addition they underpredict the experimental multiplicities. One could therefore argue that these models are incomplete and that additional processes, not included in these models, are responsible for the missing momentum. In particular, processes involving the emission of complex particles, especially α particles, may not be compatible with these models if their formation is not a simple consequence of the time evolution of the nuclear medium (coalescence, condensation, etc.). In this respect the predicted multiplicities should be closer to those observed for unbound nucleons. In the case of the NET model it should be noted that the bulk of the pre-equilibrium nucleons are emitted in the backward hemisphere due to jetting of the target nucleons through the projectile. In parentheses the values for forward jetting are given. The experimental values are based on data taken in the forward hemisphere.

It is interesting to note that the Fermi-jetting and BUU models give approximately the same value of the transferred linear momentum in spite of the fact that the proton and neutron multiplicities decrease with impact parameter much more sharply for the jetting than for the BUU calculation (see Table III). The strong dependence of the multiplicity on the impact parameter in the Fermi-jetting model is due to the decisive role of the radi-

al relative velocity in the jetting mechanism. It is seen from Table III that the agreement between the jetting and BUU models is, in a sense, only apparent because the underlying details are very different. The fact that the results of the BUU calculations are nearly independent of impact parameter may imply that the partition of the reaction channels, as obtained in the present experiment, should not depend significantly on the transferred angular momentum. Future experiments aimed at testing these predictions certainly would be of much interest. The result of the NET calculation (last entry in Table III) may indicate that the impact-parameter dependence of jetting becomes flat when nucleon-nucleon collisions are taken into account [46].

B. Energy spectra of protons

Having discussed the average characteristics of the fusionlike reactions, we examine the energy spectra of the pre-equilibrium particles and compare them with the theoretical predictions. We also address the question of complex-particle emission in fusionlike reactions.

Most of the models mentioned in this section predict energy spectra of the pre-equilibrium particles, although, as pointed out before, only the emission of nucleons and not of complex particles is taken into account. Moreover, some of the models cannot predict the angular distributions of the pre-equilibrium particles. For example, in the models based on the Boltzmann master equation

TABLE III. Impact-parameter dependence of the BUU [20], Fermi-jetting [17], and NET models [18,46].

b (fm)	l $\hbar$	BUU $\langle N_n^{pre} \rangle$	$\langle N_p^{pre} \rangle$	$\langle p \rangle/p_0$ (%)	Fermi-jetting $\langle N_n^{pre} \rangle$	$\langle N_p^{pre} \rangle$	$\langle p \rangle p_0$ (%)	NET $\langle N_n^{pre} \rangle$	$\langle N_p^{pre} \rangle$	$\langle p \rangle/p_0$ (%)
0.0	0	2.1	1.5	90	3.6	0.8	77	3.0	0.7	97
4.0	63	2.0	1.5	91	2.6	0.5	84	3.4	0.7	95
5.7	90	1.5	1.5	91	1.7	0.2	90	3.1	0.7	95
6.9	110	1.5	1.0	93	0.8	0.04	97	2.6	0.5	96
8.0	128	1.1	0.8	92	0.1	0.00	100	1.5	0.3	98
Average		1.6	1.3	91	1.7	0.3	90	2.7	0.6	96

[16] the momentum dependence is reduced to the one-dimensional energy space. Therefore, in order to compare the model predictions with the experimental results, the measured energy spectra need to be transformed to the center-of-mass system and then integrated over the entire range of emission angles. Figure 11 shows the angle-integrated multiplicity distribution of protons produced in the fusionlike collisions ($\theta_{ff} \leq 160°$). The multiplicity has been calculated relative to the number of fusionlike events. The distribution is composed of the experimental proton spectra measured in the 30 detectors of the plastic wall supplemented by the part corresponding to the angular range outside the plastic wall (both parts constituting 50% of the total), estimated by extrapolating the observed trends in the angular and energy distributions.

In Fig. 11 the predictions of three theoretical models are compared with the experimental angle-integrated spectrum of the pre-equilibrium protons. The BME calculations (solid line) have been performed by assuming that the entire projectile is captured (exciton number $n_0 = 14$) and that the full excitation energy of the composite system ($E^* = 396$ MeV) is available for the pre-equilibrium nucleon emission. The calculation was performed for a total elapsed time of 4.2×10^{-22} s (126 fm/c) which is sufficiently long to include practically all pre-equilibrium nucleons. The BUU calculation (histogram) covered a comparable time period of 125 fm/c. (The spectrum predicted by BUU has been divided by a factor of 2. The fluctuations in the computed spectrum are due to the statistical nature of the BUU calculation.) The dashed histogram in Fig. 11 shows the angle-integrated result for the NET model.

Taking into account the fact that there is no clear separation between pre-equilibrium and equilibrium (evaporation) emission, in both the experimental and theoretical results, one cannot pay much attention to the differences in shape and absolute magnitude of the multiplicity distributions at low proton energies. The differences are important, however, at higher energies where quite different exponential slopes are observed. The high-energy tail of

the calculated spectra depend strongly on the assumptions made concerning the internal momentum distribution. This aspect has been especially considered in the BUU code [20], as this influences strongly the yield of bremsstrahlung photons (from p-n collisions) and sub-threshold production of pions for which this code has been developed. In the BME model the high-energy tail of the spectrum depends on the assumed number of excitons [16]. The soft component (around 25 MeV) of the NET model is entirely due to jetting of target nucleons through the projectile, whereas the experimental data were obtained by considering the forward angular distribution only.

For the reader comparing the spectra in Fig. 11 we emphasize once again that the theoretical models considered here do not include the formation and emission of complex particles. [Explicit treatment of the complex-particle emission has been proposed on the grounds of the exciton model in several papers (see, e.g., Refs. [60,61], and references therein). These attempts were limited, however, to reactions at low energies and rather light projectiles.] The models relate the entire effect of the incomplete momentum transfer to the emission of nucleons which, in principle, may coalesce and be emitted as complex particles. One may therefore take the viewpoint that the excess observed for BME and BUU calculations accounts for the production of complex particles, mostly deuterons, tritons, and α particles. The fact that the BUU and BME calculations overpredict the experimental proton spectrum could thus be consistent with the data. Following the line of interpreting the emission of pre-equilibrium complex particles as a result of a kind of coalescence of pre-equilibrium nucleons, one can coalesce the calculated pre-equilibrium nucleon spectra and compare these with the experiment.

C. The coalescence model of complex-particle emission

Figures 12–14 show the angle-integrated spectra of deuterons, tritons, and α particles, respectively, constructed in the same way as the spectrum of protons in
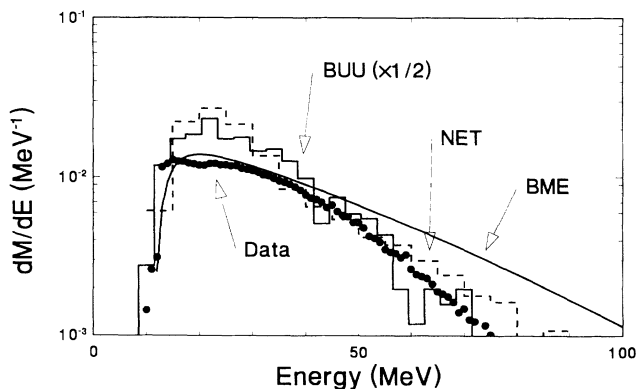

FIG. 11. Semi-inclusive, angle-integrated proton spectrum (dots) associated with fusionlike reactions. Predictions of the NET model [18], the BUU model [20] (divided by 2), and the BME model [16] are shown by the dashed line, histogram, and the solid line, respectively.
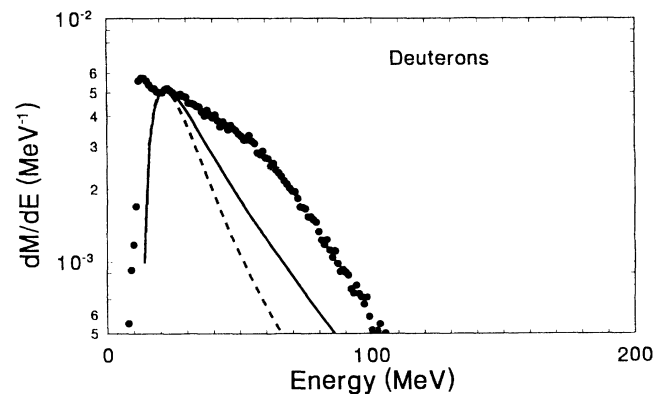

FIG. 12. Semi-inclusive deutron spectrum compared to the theoretical spectrum from coalescence of protons and neutrons obtained with the BME model [16]. The dashed curve represents the standard coalescence calculation, and the solid line shows the result of the time-sequence calculation (see text).
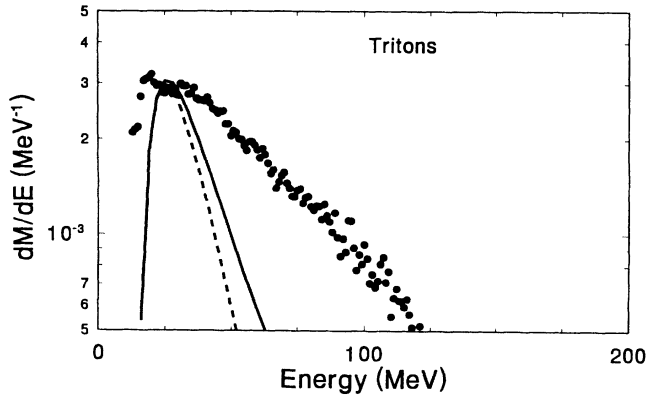
FIG. 13. Same as Fig. 12 for tritons.

Fig. 11. Again, the fusionlike processes have been selected by applying the $\theta_{ff} \leq 160°$ gate. Due to the steeper angular distributions of the complex particles, the correction for the incomplete coverage of the full solid angle turned out to be less important than for protons. For example, the correction for α particles amounts to 22% of the total α-particle yield for $\theta_{ff} \leq 160°$.

It is assumed in the coalescence model that the complex particles are formed by coalescence of the pre-equilibrium nucleons that happen to share the same volume in momentum space. The original coalescence model followed the idea of Butler and Pearson [62], and was adapted to describe the formation of complex particles in nucleus-nucleus collisions at relativistic energies [63]. Awes et al. [24] proposed a modification of the model for the range of energies at which the Coulomb repulsion plays a significant role. Note, however, that at the lower energies the physical picture of coalescence is less convincing, mostly because of the weakening correlation of the pre-equilibrium nucleons in the momentum space. There is also a decreasing coherence in the time of the particle emission. (We shall discuss this question below.) Taking all this into account, the coalescence procedure should be viewed only as a convenient tool for estimating the shapes of the energy spectra of complex particles and certainly should not be used for predicting cross sections. In fact we seriously question whether the
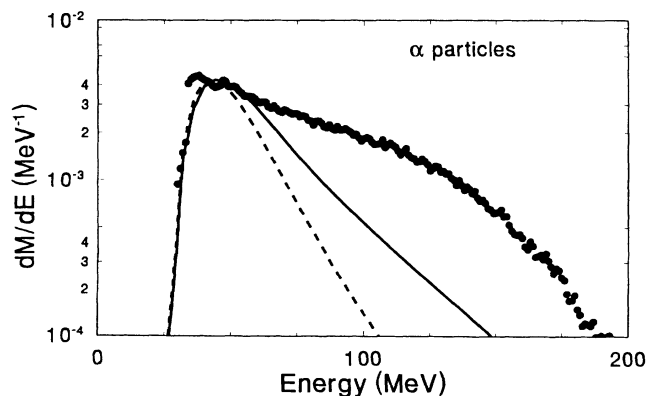
FIG. 14. Same as Fig. 12 for α's.

large observed yield of complex particles can at all be accounted for by a coalescence model without additional assumptions.

We have extended the coalescence prescription of Awes et al. [24] by allowing for the different spectral shapes of protons and neutrons (see Appendix C). Contrary to Ref. [24], in which only experimental proton spectra were used for coalescence calculations, we used the theoretical spectra of pre-equilibrium neutrons and protons, generated by the BME code, as ingredients for the calculation.

The coalescence of nucleons emitted during an extended period of time cannot be taken without reservations. The normalizing factor of the standard coalescence relation corresponds to the implicit assumption that all the nucleons produced in a given event are available at the same instant of time. From the point of view of an effective coalescence (i.e., formation of complex particles in bound states), it should be required that the particles be emitted almost simultaneously, say, at least within the time interval that is necessary for a nucleon moving with Fermi velocity to pass the distance equal to the size of the composite system (about 10^{-22} s).

Taking the above arguments into consideration, one should use the coalescence model as a description of pre-equilibrium emission of complex particles with great care. In our calculations the coalescence procedure was applied sequentially in four time intervals of 10^{-22} s by using time differential spectra from the BME code. As argued above, these intervals are short enough to assume effective coalescence within each interval. The contributions from all the four time intervals have been summed. The total elapsed time of (126 fm/c) is typical for the duration of the pre-equilibrium stage in BUU and BME calculations [20,16]. Therefore, extension of this time would not give significant additional contributions to the spectra, apart from an enhancement of the softest (evaporation) part.

Results of the coalescence calculations are shown in Figs. 12–14. Since the calculations were only used for the determination of the shape of the spectra, the calculated spectra were normalized to the data at the low-energy range. (An excess of the data at the lowest energies corresponds, most likely, to the evaporation mechanism.) In such a way, assuming that all low-energy complex particles originate from the coalescence mechanism, an upper limit on the production of pre-equilibrium complex particles due to coalescence can be established.

It is seen from Figs. 12–14 how the extension in time of the pre-equilibrium cascade influences the shapes of the predicted spectra. The solid lines have been calculated with the time-sequence method described above, while the dashed lines correspond to a standard but less realistic calculation allowing the entire (undivided) period of time. The hard part of the coalescence spectra (corresponding to the early and most intensive stage of the cascade) is relatively enhanced in the time-sequence calculation. Nevertheless, the calculated coalescence spectra of deuterons, tritons, and α particles are still much softer than the measured ones. Clearly, at the hard part of the energy spectra there is a substantial excess in the yield of

complex particles above the most optimistic predictions based on the coalescence model. There must be another reaction mechanism that contributes to the fusionlike reactions and leads to emission of complex particles.

The difference between the experimental and time differentiated coalesced BME spectra gives an approximate lower limit on the number of and energy distribution of the complex particles originating from this additional mechanism. The excess of the experimental spectra above the coalescence predictions clearly peaks at high energies, near 30 MeV/nucleon, the beam velocity. This is a characteristic feature of massive-transfer reactions in which a large fragment of the projectile is captured and only a small fragment continues with approximately the beam velocity. (The evidence that the large fragment of the projectile was indeed captured follows from the applied gate on the linear momentum transfer.)

We therefore conclude that there are two basically different reaction mechanisms that contribute to the fusionlike reactions: (i) merging of the whole projectile with the target nucleus and formation of the complete composite system that undergoes partial and later complete equilibration; and (ii) massive-transfer reactions in which a considerable part of the projectile is captured by the target nucleus, while the remaining light fragment is only a spectator in this process and continues with almost unchanged velocity.

Mechanism (i) means exactly what is assumed in the BME model and what is observed in BUU simulations when the impact parameter is not too large. The coalescence of the theoretical pre-equilibrium spectra of neutrons and protons can be used to determine the upper limit of the emission of complex particles via mechanism (i). In such a way a lower limit for the contribution of massive-transfer reactions [mechanism (ii)] to the cross section of fusionlike reactions can be established.

Table IV summarizes the results of our interpretation of fusionlike processes. Given are the average multiplicities of protons, deuterons, tritons, and α particles associated with the pre-equilibrium emission [mechanism (i)] and massive-transfer reactions [mechanism (ii)]. The multiplicities have been calculated per fission event within the fusionlike gate. It is seen that the role of the massive-transfer mechanism increases with increasing mass of the emitted complex particles. Emission of α particles in fusionlike reactions is in at least 40% of the cases due to the massive-transfer reactions.

Returning to the discussion of the average nucleonic characteristics (see Sec. V A), one can observe that the

event-averaged multiplicity of p and n associated with component (ii) is 0.4 and 0.5, respectively. The momentum that these particles carry away is about 6% of the beam momentum (i.e., assuming emission parallel to the beam direction). If these values indeed quantify mechanism (ii), then, using the experimental results of Table II, the momentum and mass balance can be used to obtain, for mechanism (i), $\langle p \rangle /p_0 = 83 + 6 = 89\%$, $\langle M_n^{\mathrm{pre}} \rangle = 3.5 - 0.5 = 3.0$, and $\langle M_p^{\mathrm{pre}} \rangle = 1.7 - 0.4 = 1.3$. These values are closer to the model predictions. One can interpret this result as an argument in support of the view that the model predictions apply only to mechanism (i) and that an additional mechanism is needed to describe the total fusionlike cross section.

VI. SUMMARY

We have determined the complete partition of the fission cross section in the $^{14}\mathrm{N} + ^{232}\mathrm{Th}$ reaction at 30 MeV/nucleon, i.e., in the energy range where the fusionlike reactions are already dominated by the processes of incomplete transfer of linear momentum, but still maintain their clear distinction from peripheral reactions (demonstrated by a deep minimum in the folding angle distribution that separates the two classes of reactions).

More than 40 different reaction channels involving nonequilibrium emission of various combinations of charged particles of multiplicity $M \leq 5$ accompanying fission events have been identified. From the measured yields the complete partition of the cross section has been deduced by solving a system of linear equations that couple the channel yields with those measured by a multidetector system (of incomplete solid-angle coverage).

For each individual channel an average value of linear momentum transfer has been determined. For reaction channels of low charged-particle multiplicity, e.g., $M = 1$, the transfer of linear momentum roughly corresponds to the kinematics of massive-transfer reactions (beam-velocity ejectiles), while for multiparticle emission ($M = 4$ and 5) the escaping particles are slower on the average. In peripheral collision they can be characterized by the kinematics of deep-inelastic reactions followed by projectile multifragmentation. An alternative (kinematical) scenario in fusionlike reactions can be represented by forward-directed multiparticle emission from a nearly thermalized composite system.

We concentrated our analysis on events that clearly originated from fusionlike reactions. Information on this

TABLE IV. Decomposition of energy-integrated multiplicites of deuterons, tritons, and α particles for fusionlike reactions into two components: Emission from the composite system [mechanism (i), upper limit] and massive-transfer reactions [mechanism (ii), lower limit]. The corresponding average kinetic energies of the particles are also given.

Ejectile	$\langle M^{\mathrm{pre}} \rangle$		$\langle E \rangle$ (MeV)	
	Mechanism (i)	Mechanism (ii)	Mechanism (i)	Mechanism (ii)
d	0.2	0.07	43	59
t	0.1	0.09	41	72
α	0.17	0.12	62	105

rather well defined class of reactions is essential for verification of existing theoretical models which, as a rule, explicitly assume the fusionlike situation as the starting point for further dynamical development of the collision process.

The results on the measured linear momentum transfer and multiplicity of pre-equilibrium particles have been compared with predictions of several models. The requirement that a theoretical model should describe simultaneously the momentum transfer and the pre-equilibrium-particle multiplicity allows one to some extent to judge the internal consistency of a model. We have found that the jetting model [17], nucleon-exchange transfer model [18], and BUU model [20] overpredict momentum transfer and underpredict the multiplicity. Therefore they are probably incomplete, i.e., additional mechanism(s) not included in the models must play a role. If only the momentum transfer is predicted correctly (leading-particle formula [48]), or even underpredicted (BME model [16]), while the multiplicity is underpredicted, the model requires some modification.

A common shortcoming of all the models is their inability to predict and describe emission of complex particles. We have found that pre-equilibrium particles emitted in the studied fusionlike reactions contain on the average $\langle M^{\mathrm{pre}} \rangle = 5.2$ nucleons, and that the multiplicity of pre-equilibrium unbound nucleons is $\langle M_p^{\mathrm{pre}} \rangle + \langle M_n^{\mathrm{pre}} \rangle = 2.6$. We addressed the question of emission of complex particles in terms of the coalescence model. The applicability of this concept for the description of time-extended pre-equilibrium processes has been discussed, and we have proposed a simple method of making the coalescence predictions more realistic from the point of view of accounting for the time scale of the pre-equilibrium nucleon emission.

We have determined an upper limit of emission of pre-equilibrium complex particles by assuming that they are formed (via coalescence) from pre-equilibrium nucleons of known (theoretical) characteristics. With the maximum possible normalization of the calculated coalescence spectra to experimental results, the data show an appreciable excess of roughly beam-velocity deuterons, tritons, and α particles. Therefore we conclude that the incomplete transfer of linear momentum that is observed in fusionlike reactions at higher energies is associated with emission of nonequilibrium nucleons and light complex particles (d, t, α) originating partly from pre-equilibrium emission from the complete composite system and partly from massive-transfer reactions in which only an incomplete composite system is formed.

ACKNOWLEDGMENTS

APPENDIX A: BUU

The BUU model calculations were made with the code described extensively in Ref. [20]. For details we refer to this article. Because the target nucleus in the present experiments is very asymmetric in isospin, the proton and neutron densities ρ_p and ρ_n differ considerably. The code was therefore adjusted on two points: For the preparation of the ground-state nuclei the local Fermi momenta were derived for protons and neutrons separately, and a symmetry potential was included. We have used

$$U_{\mathrm{sym}}(p) - U_{\mathrm{sym}}(n) = -\frac{2c}{\rho_0}[\rho_p(\mathbf{r}) - \rho_n(\mathbf{r})] \; , \qquad \text{(A1)}$$

where ρ_o is the saturation density. The constant c was adjusted in such a way that the Fermi surface of protons and neutrons in the ^{232}Th nucleus approximately coincided at -7 MeV. The value $2c = 65$ MeV was found. The simple estimate of the symmetry potential in Ref. [64] corresponds to $2c = 50$ MeV.

The calculations were performed for time steps of 0.5 fm/c and a total elapsed time of 125 fm/c, counting from the initial configuration with the surfaces of the nuclei approximately 3 fm apart. After this time a nearly spherical compoundlike nucleus had evolved for reactions with $b \leq 8$ fm. All test particles (80/nucleon) outside a radius of 11 fm ($r_0 = 1.8$ fm) in the last time step of the calculation were considered as representing pre-equilibrium particles. The parallel momenta of these test particles were added to deduce the average momentum transfer. The energy spectra were obtained by adding the potential energy to the kinetic energy of the test particles. This is only relevant for the protons (Coulomb boost), as the densities were very low in this region.

The two parameters, r_0 and the time step, thus define which particles represent equilibrium emission. In the following we discuss how the BUU results depend on these parameters.

With a smaller radius defining the residue of 9 fm ($r_0 = 1.5$ fm), the number of particles outside the residue increases significantly (by 80%). However, these additional free particles are distributed nearly symmetrically around 90°. Consequently, the momentum transfer does not change appreciably when the smaller radius is taken. Moreover, some of the test particles still had negative total energy. In general, the additional particles outside the smaller radius will add to the low-energy side of the spectrum, where they are indistinguishable from evaporated particles. Note that in a quantum-mechanical calculation, low-energy particles are partially reflected at the barrier. This effect, of course, is not present in the BUU calculation because the test particles propagate classically.

The criterion used to stop the calculations at 125 fm/c was based on the criterion for the BME code, where after 125 fm/c the cooling rate of the system has a characteristic that is expected for evaporation. Extending the calcu-

lation to 200 fm/c for $b = 5.7$ fm, we observe that the number of particles outside a radius of 11 fm increases from 3.0 to 5.3, while the momentum transfer is little affected as before. The emission rate at 200 fm/c for neutrons is approximately 2.5×10^{-3}/fm/c and is three times larger than the emission rate predicted by the BME model. For protons the rate in BUU is about 50% lower than for neutrons, while in BME the emission is negligible. As the BME model makes use of inverse cross sections to obtain the decay rates, it takes into account the quantum-mechanical aspects mentioned above. The discussion above may also illustrate the difficulties in defining a proper criterion for pre-equilibrium emission in these model calculations.

In Ref. [65] the system ^{14}N + ^{154}Sm at 35 MeV/nucleon has been studied theoretically in terms of the BUU formalism using a similar code. The same important feature has been predicted as in the present calculation for ^{14}N + ^{232}Th at 30 MeV/nucleon: Up to large impact parameters corresponding to the sum of the half-density radii, the fusionlike reactions show observables that are nearly independent of impact parameter (apart from the observables that are directly related to the angular momentum transfer). The magnitude of the momentum transfer is similar for both calculations (90%), i.e., over-predicting the observed value (83%). The particle multiplicities obtained appear much larger (12) than in the present calculation (3). However, applying the same criteria to define the number of pre-equilibrium particles (i.e., $t = 200$ fm/c, $r_0 = 1.4$ fm, and $E > 5$ MeV) we find 7.5 nucleons for the present system. The remaining difference could at least partially be due to the difference in the calculational method.

APPENDIX B: THE FERMI-JETTING CALCULATION

The closed expressions concerning momentum transfer in the Fermi-jetting model from Ref. [17] were given in-

correctly there. Expression (30) for the momentum transfer at $l = 0$ should read [66]

$$\frac{\nu}{\nu_0} = \frac{A_T(A_T - A_P)}{A^2 \nu_\infty} [\tfrac{2}{3}(1+c)(\nu_0-c)^3 - \tfrac{1}{6}c(\nu_0-c)^4 - \tfrac{1}{30}(\nu_0-c)^5] .$$

(B1)

The momentum transfer averaged over entrance angular momentum, as given in Eq. (43) of Ref. [17], has to be multiplied by a factor of 2 [66].

APPENDIX C: COALESCENCE

The coalescence formulation including protons and neutrons was derived following closely the work of Awes *et al.* [24]. The differential multiplicity spectrum for a complex particle with N neutrons and Z protons is

$$\frac{d^2N_{N,Z}(E_A)}{dE_A d\Omega} = \frac{A^{-1}}{N!Z!} \left[\frac{V_0}{\sqrt{2m^3(E-E_C)}} \right]^{A-1} \times \left[\frac{d^2N_p(E)}{dE\, d\Omega} \right]^Z \left[\frac{d^2N_n(E-E_C)}{dE\, d\Omega} \right]^N ,$$

(C1)

where $A = N + Z$, V_0 is the volume of the coalescence sphere, m is the nucleon mass, and E_C is the Coulomb energy of a proton due to the field of the emitting system. The energy of the complex particle is $E_A = AE_0 + ZE_C = AE - NE_C$, where $E = E_0 + E_C$, and E_0 is the nucleon energy at the surface of the emitting nucleus. The nucleon multiplicities are $d^2N_p(E)/dE\, d\Omega$ for protons and $d^2N_n(E)/dE\, d\Omega$ for neutrons. In the calculations, the Coulomb energy was fixed to $E_C = 10$ MeV and V_0 was adjusted to normalize the calculation to the experiment.

[1] T. Sikkeland, E. L. Haines, and V. E. Viola, Jr., Phys. Rev. **125**, 1350 (1962).

[2] B. B. Back, K. L. Wolf, A. C. Mignerey, C. K. Gelbke, T. C. Awes, H. Breuer, V. E. Viola, Jr., and P. Dyer, Phys. Rev. C **22**, 1927 (1980).

[3] M. Fatyga, K. Kwiatkowski, V. E. Viola, C. B. Chitwood, D. J. Fields, C. K. Gelbke, W. G. Lynch, J. Pochodzalla, M. B. Tsang, and M. Blann, Phys. Rev. Lett. **55**, 1376 (1985).

[4] J. M. Alexander and L. Winsberg, Phys. Rev. **121**, 529 (1961).

[5] H. Morgenstern, W. Bohne, K. Grabisch, D. G. Kovar, and H. Lehr, Phys. Lett. **113B**, 463 (1982).

[6] S. Leray, J. Phys. C **4**, 275 (1986).

[7] V. E. Viola, Jr., B. B. Back, K. L. Wolf, T. C. Awes, C. K. Gelbke, and H. Breuer, Phys. Rev. C **26**, 178 (1982).

[8] Y. Chan, M. Murphy, R. G. Stokstad, I. Tserruya, S. Wald, and A. Budzanowski, Phys. Rev. C **27**, 447 (1983).

[9] J. Jastrzebski, P. P. Singh, T. Mróz, H. J. Karwowski, S. E. Vigdor, and M. Fatyga, Phys. Lett. **136B**, 153 (1984).

[10] C. Gregoire and F. Scheuter, Phys. Lett. **146B**, 21 (1984).

[11] M. B. Tsang, D. R. Klesch, C. B. Chitwood, D. J. Fields,

C. K. Gelbke, W. G. Lynch, H. Utsunomiya, K. Kwiatkowski, V. E. Viola, Jr., and M. Fatyga, Phys. Lett. **134B**, 169 (1984).

[12] K. Aleklett, W. Loveland, M. De Saint-Simon, L. Sihver, J. O. Liljenzin, and G. T. Seaborg, Phys. Lett. B **236**, 404 (1990).

[13] J. J. Griffin, Phys. Rev. Lett. **17**, 478 (1966).

[14] M. Blann, Phys. Rev. Lett. **27**, 337 (1971).

[15] E. Gadioli and E. Gadioli-Erba, Nucl. Instrum. Methods **146**, 265 (1977).

[16] M. Blann, Phys. Rev. C **31**, 1245 (1985).

[17] K. Möhring, W. J. Swiatecki, and M. Zielinska-Pfabé, Nucl. Phys. **A440**, 89 (1985).

[18] J. Randrup and R. Vandenbosch, Nucl. Phys. **A474**, 219 (1987).

[19] G. F. Bertsch and S. Das Gupta, Phys. Rep. **160**, 189 (1988).

[20] W. Cassing, V. Metag, U. Mosel, and K. Niita, Phys. Rep. **188**, 363 (1990).

[21] H. C. Britt and A. R. Quinton, Phys. Rev. **124**, 877 (1961).

[22] T. Inamura, M. Ishihara, T. Fukuda, T. Shimoda, and H. Hiruta, Phys. Lett. **68B**, 51 (1977).

[23] K. Siwek-Wilczyńska, E. H. du Marchie van Voorthuysen, J. van Popta, R. H. Siemssen, and J. Wilczyński, Phys. Rev. Lett. 42, 1599 (1979).

[24] T. C. Awes, G. Poggi, C. K. Gelbke, B. B. Back, B. G. Glagola, H. Breuer, and V. E. Viola, Phys. Rev. C 24, 89 (1981).

[25] G. J. Balster, R. H. Siemssen, and H. W. Wilschut, Nucl. Phys. A471, 635 (1987).

[26] C. B. Chitwood, D. J. Fields, C. K. Gelbke, D. R. Klesch, W. G. Lynch, M. B. Tsang, T. C. Awes, R. L. Ferguson, F. E. Obenshain, F. Plasil, R. L. Robinson, and G. R. Young, Phys. Rev. C 34, 858 (1986).

[27] B. V. Jacak, G. D. Westfall, G. M. Crawley, D. Fox, C. K. Gelbke, L. H. Harwood, B. E. Hasselquist, W. G. Lynch, D. K. Scott, H. Stöcker, M. B. Tsang, G. Buchwald, and T. J. M. Symons, Phys. Rev. C 35, 1751 (1987).

[28] P. C. N. Crouzen, Ph.D. thesis, Rijks Universiteit Groningen, Kernfysisch Versneller Instituut, 1988.

[29] E. E. Koldenhof, R. van de Ploeg, and H. W. Wilschut, Kernfysisch Versneller Instituut Groningen, Annual Report, 1986, p. 132.

[30] H. K. W. Leegte, E. E. Koldenhof, A. L. Boonstra, and H. W. Wilschut, Nucl. Instrum. Methods A313, 26 (1992).

[31] LeCroy Model 4300B.

[32] M. B. Tsang, C. B. Chitwood, D. J. Fields, C. K. Gelbke, D. R. Klesch, W. G. Lynch, K. Kwiatkowski, and V. E. Viola, Phys. Rev. Lett. 52, 1967 (1984).

[33] M. Fatyga, K. Kwiatkowski, V. E. Viola, W. G. Wilson, M. B. Tsang, J. Pochodzalla, W. G. Lynch, C. K. Gelbke, D. J. Fields, C. B. Chitwood, Z. Chen, and T. Nayak, Phys. Rev. Lett. 58, 2527 (1987).

[34] J. B. Natowitz, E. T. Chulick, and M. N. Namboodiri, Phys. Rev. C 6, 213 (1972).

[35] J. Galin, D. Guerreau, M. Lefort, and X. Tarrago, Phys. Rev. C. 9, 1018 (1974).

[36] D. Glass and U. Mosel, Nucl. Phys. A237, 429 (1975).

[37] D. J. Morrissey, G. J. Wozniak, L. G. Sobotka, R. J. McDonald, A. J. Pacheco, and L. G. Moretto, Nucl. Phys. A442, 578 (1985).

[38] V. E. Viola, K. Kwiatkowski, and M. Walker, Phys. Rev. C 31, 1550 (1985).

[39] J. C. Steckmeyer, F. Lefebvres, C. Lebrun, J. F. Lecolley, M. L'Haridon, A. Osmont, and J. P. Patry, Nucl. Phys. A427, 357 (1984).

[40] R. K. Bhowmik, J. van Driel, R. H. Siemssen, G. J. Balster, P. B. Goldhoorn, S. Gonggrijp, Y. Iwasaki, R. V. F. Janssens, H. Sakai, K. Siwek-Wilczyńska, W. A. Sterrenburg, and J. Wilczyński, Nucl. Phys. A390, 117 (1982).

[41] J. van Driel, S. Gonggrijp, R. V. F. Janssens, R. H. Siemssen, K. Siwek-Wilczynska, and J. Wilczynski, Phys. Lett. 98B, 351 (1981).

[42] W. D. M. Rae, A. J. Cole, B. G. Harvey, and R. G. Stokstad, Phys. Rev. C 30, 158 (1984).

[43] C. Pruneau, L. Potvin, R. Roy, C. St. Pierre, G. C. Ball, R. Bougault, E. Hagberg, D. Horn, D. Cebra, D. Fox, and G. D. Westfall, Nucl. Phys. A500, 168 (1989).

[44] E. E. Koldenhof (unpublished).

[45] A. Chbihi, L. G. Sobotka, Z. Majka, D. G. Sarantites, D. W. Stracener, V. Abenante, T. M. Semkow, N. G. Nicolis, D. C. Hensley, J. R. Beene, and M. L. Halbert, Phys. Rev. C 43, 652 (1991).

[46] R. Vandenbosch, private communication.

[47] G. D. Harp, J. M. Miller, and B. J. Berne, Phys. Rev. 165, 1116 (1968).

[48] J. B. Natowitz, S. Leray, R. Lucas, C. Ngô, E. Thomasi, and C. Volant, Z. Phys. A 325, 467 (1987).

[49] J. Aichelin, in The Nuclear Equation of State. Part A: Discovery of Nuclear Shock Waves and the EOS, edited by W. Greiner and H. Stöcker (Plenum, New York, 1989).

[50] T. Maruyama, A. Ohnishi, and H. Horiuchi, Phys. Rev. C 42, 386 (1990).

[51] D. H. Boal and I. C. K. Wong, Phys. Rev. C 41, 118 (1990).

[52] E. Holub, D. Hilscher, G. Ingold, U. Jahnke, H. Orf, and H. Rossner, Phys. Rev. C 28, 252 (1983).

[53] E. Holub, D. Hilscher, G. Ingold, U. Jahnke, H. Orf, H. Rossner, W. P. Zank, W. U. Schroder, H. Gemmeke, K. Keller, L. Lassen, and W. Lucking, Phys. Rev. C 33, 143 (1986).

[54] W. P. Zank, D. Hilscher, G. Ingold, U. Jahnke, M. Lehmann, and H. Rossner, Phys. Rev. C 33, 519 (1986).

[55] A. Gavron, A. Gayer, J. Boissevain, H. C. Britt, T. C. Awes, J. R. Beene, B. Cheynis, D. Drain, R L. Ferguson, F. E. Obenshain, F. Plasil, G. R. Young, G. A. Petitt, and C. Butler, Phys. Rev. C 35, 579 (1987).

[56] D. Hilscher, H. Rossner, A. Gamp, U. Jahnke, B. Cheynis, B. Chambon, D. Drain, C. Pastor, A. Giorni, C. Morand, A. Dauchy, P. Stassi, and G. Pettit, Phys. Rev. C 36, 208 (1987).

[57] G. Mantzouranis, H. A. Weidenmüller, and D. Agassi, Z. Phys. A 276, 145 (1976).

[58] M. Blann, W. Scobel, and E. Plechaty, Phys. Rev. C 30, 1493 (1984).

[59] M. Blann, Phys. Rev. C 31, 295 (1985).

[60] A. Iwamoto and K. Harada, Nucl. Phys. A419, 472 (1984).

[61] J. Bisplinghoff and H. Keuser, Phys. Rev. C 35, 821 (1987).

[62] S. T. Butler and C. A. Pearson, Phys. Rev. 129, 863 (1963).

[63] H. H. Gutbrod, A. Sandoval, P. J. Johansen, A. M. Poskanzer, J. Grosset, W. G. Meyer, G. D. Westafall, and R. Stock, Phys. Rev. Lett. 37, 667 (1976).

[64] A. Bohr and B. R. Mottelson, Nuclear Structure (Benjamin, New York, 1969), Vol. 1, pp. 146–149.

[65] M. B. Tsang, G. F. Bertsch, W. G. Lynch, and M. Tohyama, Phys. Rev. C 40, 1685 (1989).

[66] K. Möhring, private communication.